Delay Skew Packet Flow Control in Wireless Systems with Dual Connectivity

Torbjörn Wigren, *Senior Member IEEE*, Katrina Lau, *Member IEEE*, Ramon Delgado , and Richard H. Middleton, *Fellow IEEE*

***Abstract*—The paper presents a new data flow controller for use in 4G and 5G wireless applications where the incoming internet data flow is split in support of multi-point downlink wireless transmission. The different paths of the data from the node of the split to the wireless transmission nodes and on to the mobile may then result in different travel times. The mobile can cope with small values of this delay skew by means of buffers and re-ordering protocols. The control objective is therefore to keep the delay skew within a pre-specified interval of time, when the packets arrive in the mobile. The proposed algorithm solves the problem by cascade control. The packet dwell time of each wireless transmission node data queue is controlled by an inner loop, with the reference dwell times being determined by an outer delay skew control loop. The delay skew control loop exploits a deadzone to achieve interval control. In a further contribution the $\mathcal{L}_2$-stability of the controller is analyzed for the dual connectivity functionality of the coming 5G cellular network deployment. A combined use of the input-output Nyquist- and Popov-criteria is required for the analysis. The performance is also evaluated by a laboratory testbed implementation.**

***Index Terms*—4G, 5G, Wireless, Delay, Internet of Things, MIMO Control, Networked Control, Stability.**

I. Introduction

THE internet of things (IoT) is expected to grow rapidly when the new fifth generation (5G) wireless standards are introduced [6], [21]. Some of the new IoT applications will require remote control over the wireless interfaces, which puts networked control systems (NCS) at the focal point [1]. Some expected applications include e.g. automotive safety, remote surgery and manufacturing plants with feedback controlled industrial robots. In the past, a weak point of cellular wireless systems has been their high latency, a fact that is addressed in the ongoing 5G wireless standardization. However, it is foreseen that delay tolerant networked control will remain a critical component in this equation, which is one reason why a renewed focus on delay in control was called for in [22]. Here the underlying packet flow controller algorithm that controls the latency between the controlling node and the node of the plant is of paramount importance. It is stressed that the delay control algorithm needs to guarantee the latency despite disturbances caused by fading radio connections [11] and internet connection delay variations [25].

In 5G wireless systems the carrier frequencies will increase beyond 10 GHz, which leads to increased radio shadowing. This means that downlink transmission from multiple wireless transmission nodes will be needed to achieve a sufficient coverage and robustness [6], [21], [31]. Other reasons for multi-point access include capacity enhancements using coordinated wireless transmission schemes, [3]. One consequence of the above facts is a need for the wireless community to address the details of delay control between different transmission points. For example, in case the multi-point transmissions are not properly delay skew controlled, coordinated wireless transmission schemes may become less efficient. In addition, several new 5G use cases require such delay control, among these ultra-reliable multi-point transmission for machine type communication where diversity gains are to be obtained by simultaneous transmission of the same data from multiple transmission nodes. Put otherwise, without efficient end-to-end delay control, parts of the advantages of the 5G wireless interfaces may be lost in other parts of the signal chain. A main purpose with this publication is therefore to contribute to a closer integration of techniques from control and communication, to obtain competitive solutions to the challenging 5G wireless radio conditions and use cases.

A consequence of multi-point transmission is thus that incoming data streams will be split over different paths to the receiving end users. As stated above, new data flow control algorithms are then needed to ensure that the delay differences between different paths are kept within acceptable limits. These delay differences are denoted delay skews. The paper hence assumes that there is a controlling node, where the incoming data stream from the application is split into one data flow to each of the transmission nodes. Each of these data flows exploits a separate so called backhaul connection [25]. The requirements on the delay skew controller treated in the present paper are:

- The down link delay skew from the controller to the wireless interfaces should remain in a specified range.
- The transmit data queue dwell times should be controlled to avoid wireless data starvation, whilst maintaining low dwell times.
- The delay skew control algorithm should be globally stable.
- The computational complexity should be small.

The first requirement is needed to address the delay skew

T. Wigren is with L5GR Systems, Ericsson AB, Stockholm, SE-16480 Sweden. e-mail: torbjorn.wigren@ericsson.com.

R. Delgado, K. Lau and R. H. Middleton are with the Centre for Dynamic Systems and Control, The University of Newcastle, Callaghan, NSW 2308, AUSTRALIA. e-mail: {ramon.delgado, k.lau, richard.middleton } @newcastle.edu.au .

Manuscript received October 10, 2016.

Peer-reviewed author's copy of:
T. Wigren, K. Lau, R.A. Delgado and R. H. Middleton. **Delay Skew Packet Flow Control in Wireless Systems With Dual Connectivity**. In *IEEE Transactions on Vehicular Technology*, vol. 67, no. 6, pp. 5357-5371, June 2018.
Available at https://doi.org/10.1109/TVT.2018.2808533

control use case and to be consistent with the re-ordering depth configuration of the mobile [10], while the second requirement ensures that wireless capacity is not wasted. This clearly requires delay skew regulation consistent with the variation of the wireless data rates, so that the buffering of the transmission nodes continue to operate as intended. The stability requirement is needed to guarantee the performance of the delay skew controller at all times, a fact that cannot be compromised in commercial deployments. Since the number of controller instances may reach several thousands in a single controlling node, low computational complexity is another pre-requisite.

The standard packet flow control techniques that may provide delay control over the 5G wireless and wired internet include the transmission control protocol (TCP). TCP has been further developed in a number of variants and augmentations, like the recent bottleneck bandwidth and round trip time (BBR) congestion control algorithm [2]. TCP has also been augmented with active queue management (AQM) algorithms, see e.g. [25]. TCP aims for capacity optimization, while AQM is based on packet discards to mitigate problems with queue data volume overflow with less delay than TCP. However, TCP and AQM typically build on irregular acknowledgment / not acknowledgement (ACK/NACK) feedback to the internet data source. Therefore TCP and AQM cannot provide as accurate delay control as an algorithm located closer to the end user mobile, that processes regularly sampled delay feedback measurements to control the delay properties of the data paths between the controller and the mobile. The delay control problem may be hard even for such a controller because of the rapidly varying radio channel fading and data rates [11], together with the loop delay itself. Note that the required feedback tends to consume parts of the capacity, which is a price that needs to be paid to achieve improved delay properties.

The main scope of the present paper is to develop a delay skew controller that meets the four requirements listed above. Towards this end, the first contribution suggests a new interval delay skew control objective that is defined and measured between the controlling node and the downlink wireless interfaces of the transmission nodes. The objective addresses the first requirement above. To meet the requirement of a low computational complexity, advanced nonlinear design methods like model predictive control [12] are abandoned in favor of a cascade control architecture. This second contribution uses low complexity inner control loops [27] - [30], that manipulate the downlink backhaul data rates to control the transmit data queue dwell times according to dwell time reference values computed by an outer delay skew control loop. The inner loops of the delay skew controller thereby determine the instantaneous backhaul data flow rates, which fully define the split of the data flow. The non-linear dynamic data flow split problem is thereby circumvented and instead solved by almost linear delay control means. Input-output stability is then analysed in the third contribution using a novel combination of the Nyquist- and Popov-criteria [26], under the assumption that the inner loops operate as intended, as secured by the stability analysis of [27] - [30]. The fourth requirement is met since the proposed controller structure is a linear one, with a deadzone added for interval control. The fifth contribution treats the performance of the controller in a dual connectivity setup, by a closed loop analysis of linear disturbance rejection properties and by experiments with a production test bed C++ implementation. It is stressed that the paper treats a delay control use case, with other primary requirements than the traditional mobile broadband use case. Therefore the numerical evaluation is not focused on capacity.

Much of the research in the past few decades on networked control has been concerned with quantization and the associated data rate theorems [1]. The present paper is however instead focused on the effect of delay. The wireless delay skew control application of this paper is believed to be new, with further results reported by the same authors in [4], [5], [15], [16] and [18]. The more advanced stability analysis provided by the integral quadratic constraint (IQC) theory of [14] and [17] provide the tools needed for a generalization of the present stability results to an arbitrary number of wireless transmission nodes in [5]. This analysis is based on a general static decoupling described in [15]. The IQC stability results are however obtained numerically and lacks the intuitive and graphical frequency domain interpretations that are possible in the two-node case of the present paper. In addition the analysis of [5] treats the different case with non-negativity of the inner loop delay reference values. The paper [16] is an exception from the need to use IQC to analyze delay skew control stability for an arbitrary number of transmission nodes. The simplification of the outer loop of that paper leaves only the inner loop dynamics, which can be treated by a repeated application of the Popov criterion, building on results of [27]. The papers [4] and [18] solve the related problem of controlling the *round trip delay skews* over multiple wireless interfaces, while the present paper aims to control the *downlink delay skew* to the wireless interface in the transmission nodes. The controllers of [4] and [18] therefore provide guaranteed loop delays for application layer feedback controllers using so called ultra reliable low latency communications (URLLC), while the controller of the present paper provides guaranteed in time delivery of data to the mobile over multiple transmission paths, suitable e.g. for video streaming. The difference may appear to be subtle, however the two objectives require radically different inner loop controllers and measurements, with large differences resulting in the stability analysis. It should be noted that there is also a significant amount of research on single leg flow control that is related to the present work, see e.g. [13], [24], [27] - [30]. The vast literature on control and stability of systems with delay cannot be reviewed here, but needs to be kept in mind when further research is conducted.

The paper is organized with the theoretical stability aspects treated in section III. The intention is that readers without a background in feedback stability theory should be able to get a self-contained treatment of the engineering ideas without reading this part. Hence, the delay skew controller is developed in Section II. The reference tracking and disturbance rejection properties are then discussed in section IV. Numerical results follow in Section V and the paper is concluded in Section VI.

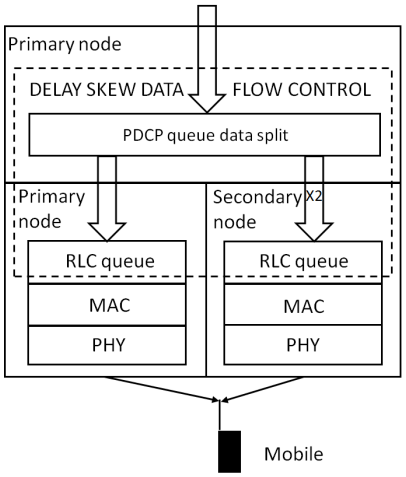

Fig. 1. The dual connectivity architecture. The LTE protocol specifications of the Figure include: PDCP [9], radio link control (RLC) [10], medium access control (MAC) [7] and physical layer (PHY) [8]. The PDCP split bearer architecture of DC release-12 appears in [23].

II. Interval Delay Skew Packet Flow Control

A. Mobile Broadband Flow Control with Dual Connectivity

One starting point for multi-point 5G wireless transmission is the so called dual connectivity (DC) functionality. DC was introduced in release-12 of the long term evolution (LTE) fourth generation (4G) cellular system [3], [23], and it aggregates connectivity from multiple transmission resources that may belong to different radio access technologies like 4G LTE and future 5G wireless access. The architecture is depicted in Fig. 1. Since the 5G standards are in development, the DC functionality for the 4G LTE system is described here.

The incoming data stream from an internet source is split at the packet data convergence protocol (PDCP) layer. The protocol data units (PDUs) are then sent to the mobile either via a master cell group (MCG), or via a secondary cell group (SCG). In the setup of Fig. 1 one stream of data is transmitted directly to the UE by its primary node. The second stream of data is sent over the X2 interface of LTE to the secondary node from which the data is transmitted to the UE. The X2 interface forms the backhaul and it may be implemented in many ways, e.g. using fibre or wireless backhaul [20]. Some of these technologies can result in substantial delay that may not be precisely known. Since the re-ordering buffers in the mobile can only handle a limited time interval, the conclusion is that delay skew packet flow control is needed in the downlink, between the primary and the secondary nodes.

In Fig. 1 the controlling node is located at the PDCP layer of the primary node of the dual connectivity architecture, whereas the wireless transmission nodes correspond to the RLC, MAC and PHY layers of the primary and secondary nodes. It can be noted that the flow control loop that is a part of the primary node is usually significantly faster than the one between the primary and secondary node, and in some implementations it may not be needed at all. In this paper, however, it is assumed that primary node flow control is present.

B. Interval Delay Skew Controller Block Diagram

The delay skew controller for the two-node dual connectivity architecture is depicted in Fig. 2. The idea is to apply cascade control. The outer delay skew control loop measures the delay skew between the two transmission nodes, counted from the data split point to the downlink wireless interface. This delay skew feedback measurement, together with a corresponding feedback measurement of the sum of the delays, are then used for control of the reference values of the inner loops. The inner loops control the dwell time of the transmit data queues of each transmission node, by variation of the data volume of the queues using the downlink backhaul data rate control signals [27] - [30]. These queues provide the needed buffering to ensure that the wireless interfaces are not subject to data starvation caused by the combination of the backhaul delay and the rapidly varying radio channel capacity that is caused by fading and shadowing [11], [21], [31]. It is important to note that the inner loop control signals, i.e. the downlink backhaul data rates, fully define the data flow split at the controlling node. The delay skew controller thereby also solves the data flow split problem at the controlling node. It does so by using the downlink data flows themselves in order to control the total downlink delays, from the controlling node to the wireless interfaces. As stated above the delay skew need not be controlled to exactly zero since the communication protocols are able to perform packet re-ordering in case the arrival times of originally adjacent packets differ by less than the re-ordering buffer length. This re-ordering buffer may be of the order of 20 ms [10]. This is the reason for the delay skew interval control that is represented by the deadzone in Fig. 2.

Approximations are needed in order to meet the objective to have a low computational complexity. These approximations are introduced in the following detailed description of the delay skew control loop. The control objective is represented by $T_{skew}^{ref}(s)$, where s is the independent variable of the Laplace transform. There also needs to be a corresponding reference value $T_{sum}^{ref}(s)$ for the sum of the delays, to ensure that the absolute delay does not become too large. Both $T_{skew}^{ref}(s)$ and $T_{sum}^{ref}(s)$ can be selected as constants, this is e.g. the case in section V of the paper. The control errors

$$e_{skew}(s) = T_{skew}^{ref}(s) - T_{skew}(s), \tag{1}$$

$$e_{sum}(s) = x_2(s) = T_{sum}^{ref}(s) - T_{sum}(s) \tag{2}$$

are then formed, where $T_{skew}(s)$ and $T_{sum}(s)$ denote the delay skew and delay sum feedback signals. Next, the corresponding time domain skew control error $e_{skew}(t)$ is fed through the deadzone to give

$$x_1(t) = \begin{cases} e_{skew}(t) - \Delta T_{skew}, & e_{skew}(t) > \Delta T_{skew} \\ 0.0, & |e_{skew}(t)| \leq \Delta T_{skew} \\ e_{skew}(t) + \Delta T_{skew}, & e_{skew}(t) < -\Delta T_{skew}. \end{cases} \tag{3}$$

The size of the deadzone is hence given by $\Delta T_{skew} \geq 0$. The outer loop control signals are obtained as

$$u_{skew}(s) = C_{skew}(s)x_1(s), \tag{4}$$

$$u_{sum}(s) = C_{sum}(s)x_2(s), \tag{5}$$

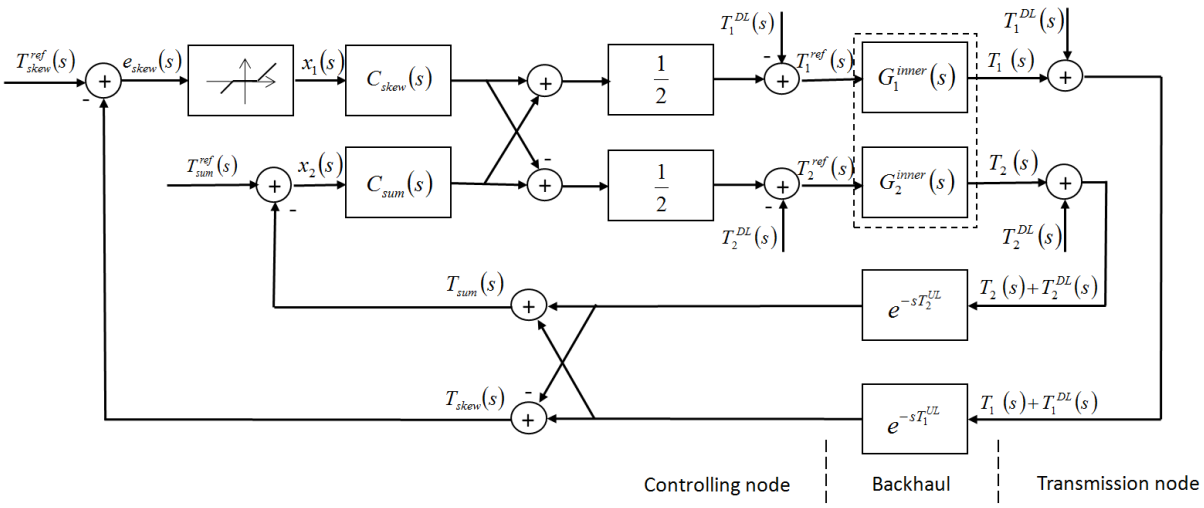

Fig. 2. The two node downlink delay skew controller block diagram. Block diagrams for the inner loops (dashed) appear in [27] and [28]-[30].

where the feedback controller filters are given by $C_{skew}(s)$ and $C_{sum}(s)$. There are many ways to design the controller filters with a static nonlinearity in the loop, see e.g. [27]-[30] for lead-lag-, LQG- ,H_∞-, and H_2-design techniques, respectively. The control signals need some further transformation in order to obtain the reference values for the inner control loops. Straightforward calculations in a static situation, assuming that the outer loop reference values are achieved, leads to the conclusion that the reference values are obtained by the following transformations

$$T_1^{ref}(s) = \frac{1}{2}\left(u_{skew}(s) + u_{sum}(s)\right) - T_1^{DL}(s), \qquad (6)$$

$$T_2^{ref}(s) = \frac{1}{2}\left(u_{sum}(s) - u_{skew}(s)\right) - T_2^{DL}(s). \qquad (7)$$

In (6) and (7), the subtraction of the backhaul delays $T_1^{DL}(s)$ and $T_2^{DL}(s)$ follows since the inner loop controllers are designed for control of the dwell time of the data packets in the transmit data queues of the wireless transmission nodes, exclusive of the backhaul interface delays. Note that the static decoupling of the control channels provided by (6) and (7) can be systematically extended to any number of transmission nodes, see [4].

Next the inner loop controllers need to be discussed. These controllers apply feedback from the transmit queue data volume and optionally feed-forward from the scheduled wireless rate. The dwell time control is obtained by a reference value transformation from a dwell time reference to a data volume reference, using the wireless rate, see [27]. The dwell time control is therefore obtained by a combination of the reference value transformation and the transmit data queue volume feedback control. The inner loops of [27]-[30] are also subject to a saturation since the flow of data is one-directional. The inner loop modeling of this paper assumes that the loops operate as intended so that the saturation can be neglected. This is motivated by the cascade control approach taken in the paper. In addition it is assumed that the effect of the reference value transformation allows modeling of the queue dwell times by time invariant models, as indicated by Fig. 2. Irrespective of the technique applied, the inner feedback loops can then be characterized by loop gains $\hat{g}_i(s)$, defined excluding the delays. Referring to [27] and the block diagram therein, the inner loops can be modeled as follows in case of lead-lag control or in case of any other controller where the inner loop feedback controller filter $F_{y,i}(s)$ operates on the feedback control error:

$$G_i^{inner}(s) = \frac{G_{0,i}\hat{g}_i(s)e^{-sT_i^{DL}}}{1 + \hat{g}_i(s)e^{-s(T_i^{DL}+T_i^{UL})}}, \ i = 1, 2. \qquad (8)$$

Here T_i^{DL} and T_i^{UL}, $i = 1, 2$, are the *nominal* downlink and uplink delays that are introduced in order to obtain linear time invariant models of the inner loops. In practice the nominal delays need to be selected based on prior knowledge or as time averages obtained from on-line or off-line measurements. The nominal delays can be thought of as the typical delays of the backhaul downlink and the backhaul uplink. Their introduction is required for inner loop controller design and for the analysis of the stability and disturbance rejection properties later in the paper. Technically, the reason is the delay operators $e^{-s(\cdot)}$ of Fig. 2 need constant delays as their argument. Note that the dynamic backhaul delay effects are captured by $T_i^{DL}(s)$ and $T_i^{UL}(s)$, $i = 1, 2$, whenever that is possible without violation of linearity and time invariance. The modeling is hence a compromise that requires the inner loop transfer functions to be based on nominal fixed backhaul delays.

The dynamic effect of the transmit data queue becomes embedded in $\hat{g}_i(s)$, $i = 1, 2$, see [27]. In the case of state feedback control as in [28]-[30], the corresponding dynamic models of the inner loops become

$$G_i^{inner}(s) = \frac{G_{0,i}\hat{g}_i(s)(F_{y,i}(s))^{-1}e^{-sT_i^{DL}}}{1 + \hat{g}_i(s)e^{-s(T_i^{DL}+T_i^{UL})}}, \ i = 1, 2. \qquad (9)$$

See [28]-[30] for the block diagrams underpinning (9). These block diagrams reveal the reason why $F_y(s)$ appears in (9) and not in (8). The reason is that the lead-lag controller operates directly on the control error, while the state space

control algorithms operate on estimated states. Furthermore $G_{0,i},\ i = 1,2$ of (8) and (9) represent the reference signal gains that are used to adjust the overall static gains of the inner loops. Exact relations for the loop gains $\hat{g}_i(s)$, $i = 1,2$, can be obtained from [27]-[30]. An example appears in Section V of this paper.

The output signal from the inner control loops are the transmit queue dwell times of each transmission node, i.e. $T_i(s),\ i = 1,2$. Addition of the downlink backhaul delays as shown in Fig. 2 give the total downlink delays from the point where the data split occurs, to the wireless interface of each transmission node. These signals are then sent over the backhaul interface back to the controlling node, where they are combined into the delay skew and the delay sum signals

$$T_{skew}(s) = e^{-sT_1^{UL}}\left(T_1(s) + T_1^{DL}(s)\right) - e^{-sT_2^{UL}}\left(T_2(s) + T_2^{DL}(s)\right), \quad (10)$$

$$T_{sum}(s) = e^{-sT_1^{UL}}\left(T_1(s) + T_1^{DL}(s)\right) + e^{-sT_2^{UL}}\left(T_2(s) + T_2^{DL}(s)\right). \quad (11)$$

C. Interval Delay Skew Controller State Space Model

To derive a state space model representing the control system of Fig. 2, the treatment of the inner control loops as seen by the outer control loop needs to be further discussed. The following assumptions, some of which have already been introduced, are needed for the inner control loops:

- A1) The data rate saturation of the inner control loops can be neglected.
- A2) The input and output transformations of the inner control loops, from time to queue data volume and back, can be neglected.
- A3) Disturbances and feed-forward signals of the inner control loops can be neglected.
- A4) The reference values $T_i^{ref}(t) \geq 0.0$, $i = 1,2$.

It can be noted that A1 - A4 are inspired by the widely accepted cascade control paradigm, i.e. the assumption that the inner loops operate faster and in line with the reference values provided by the outer delay skew control loop. The assumption A1 is supported by the simulations of [27]-[30], that show that data rate saturation typically only occurs after a transmit queue overflow situation. The assumption A2 can also be expected to be valid since the outer delay skew control loop should have a significantly lower bandwidth than the inner loops. This fact makes it reasonable to assume a time invariant linear model for the inner loops, within the outer loop bandwidth. A3 is concerned with the inner loop external signal properties and these were discussed and found reasonable in [27]-[30]. The assumption A4 is needed to allow an analysis with the single-input-single-output (SISO) Popov criterion [26], since otherwise saturations would be needed at the input to both inner control loops. In practice A4 can be enforced by increasing the total delay budget represented by $T_{sum}^{ref}(s)$. This is not a limitation in practical applications, since active positivity limitations on the queue dwell time references would mean that delay skew control loop inconsistencies have occurred. In case A4 is removed, the more advanced IQC techniques could be used for a refined stability analysis [14], [17].

Straightforward calculations using Fig. 2 results in the following state space model for the linear parts of the delay skew control loop

$$\begin{pmatrix} T_{skew}(s) \\ T_{sum}(s) \end{pmatrix} = \begin{pmatrix} A_{11}(s) & A_{12}(s) \\ A_{21}(s) & A_{22}(s) \end{pmatrix} \begin{pmatrix} x_1(s) \\ x_2(s) \end{pmatrix} + \begin{pmatrix} B_{11}(s) & B_{12}(s) \\ B_{21}(s) & B_{22}(s) \end{pmatrix} \begin{pmatrix} T_1^{DL}(s) \\ T_2^{DL}(s) \end{pmatrix} = \mathbf{A}(s) \begin{pmatrix} x_1(s) \\ x_2(s) \end{pmatrix} + \mathbf{B}(s) \begin{pmatrix} T_1^{DL}(s) \\ T_2^{DL}(s) \end{pmatrix}. \quad (12)$$

Here

$$A_{11}(s) = \frac{1}{2} C_{skew}(s) \left(e^{-sT_1^{UL}} G_1^{inner}(s) + e^{-sT_2^{UL}} G_2^{inner}(s) \right), \quad (13)$$

$$A_{12}(s) = \frac{1}{2} C_{sum}(s) \left(e^{-sT_1^{UL}} G_1^{inner}(s) - e^{-sT_2^{UL}} G_2^{inner}(s) \right), \quad (14)$$

$$A_{21}(s) = \frac{1}{2} C_{skew}(s) \left(e^{-sT_1^{UL}} G_1^{inner}(s) - e^{-sT_2^{UL}} G_2^{inner}(s) \right), \quad (15)$$

$$A_{22}(s) = \frac{1}{2} C_{sum}(s) \left(e^{-sT_1^{UL}} G_1^{inner}(s) + e^{-sT_2^{UL}} G_2^{inner}(s) \right), \quad (16)$$

$$B_{11}(s) = e^{-sT_1^{UL}}\left(1 - G_1^{inner}(s)\right), \quad (17)$$

$$B_{12}(s) = -e^{-sT_2^{UL}}\left(1 - G_2^{inner}(s)\right), \quad (18)$$

$$B_{21}(s) = e^{-sT_1^{UL}}\left(1 - G_1^{inner}(s)\right), \quad (19)$$

$$B_{22}(s) = e^{-sT_2^{UL}}\left(1 - G_2^{inner}(s)\right). \quad (20)$$

III. $\mathcal{L}_2$ Stability

To analyse the control system, the first step is to establish conditions for stability. This then motivates the continued evaluation of reference tracking and disturbance rejection performance in the following section. Readers unfamiliar with stability analysis can e.g. read Theorem 1 and treat the remaining parts of this section as an annex providing proofs.

The stability analysis needs to be based on input-output stability methods, since the delays of the backhaul make the control system infinite dimensional. Therefore $\mathcal{L}_2$-stability as discussed in [26] is applied here. Since there is only a single nonlinearity to account for, the strategy is to reduce the multiple-input-multiple-output (MIMO) block diagram of Fig. 2 into the scalar block diagram of Fig. 3, with a resulting loop gain in cascade with the deadzone. This loop gain also accounts for the dynamic effect of the sum of delays loop. The

details of the transformations that map Fig. 2 onto Fig. 3 are obtained by straightforward algebraic manipulations in section III.D. To be able to use the Popov-criterion for analysis of the non-linear loop, the loop gain needs to be internally $\mathcal{L}_2$-stable, a fact which explains the occurrence of the Nyquist-criterion in the main result below.

A. Definitions, the Nyquist criterion and the Popov Criterion

The following definitions that appear in [26] define the concept of $\mathcal{L}_2$-stability.

Definition 1: For all $p \in [1, \infty)$, $\mathcal{L}_p[0, \infty)$ denotes the set of all measurable functions $f(\cdot) : [0, \infty) \to \mathcal{R}$, such that

$$\|f(\cdot)\|_p^p = \int_0^\infty |f(t)|^p dt < \infty.$$

Definition 2: The set of all measurable functions $f(\cdot) : [0, \infty) \to \mathcal{R}$, such that their truncations

$$f_T(t) = \begin{cases} f(t), & 0 \le t \le T \\ 0, & t > T \end{cases} \in \mathcal{L}_p[0, \infty),$$

$\forall T$, is denoted the extension $\mathcal{L}_{pe}[0, \infty)$ of $\mathcal{L}_p[0, \infty)$.

Definition 3: The mapping $A : \mathcal{L}_{pe} \to \mathcal{L}_{pe}$ is $\mathcal{L}_p$-stable if i) $Af \in \mathcal{L}_p$ whenever $f \in \mathcal{L}_p$, and ii) there exist finite constants l, c, such that

$$\|Af\|_p \le l\|f\|_p + c, \quad \forall f \in \mathcal{L}_p.$$

Definition 4: $\mathcal{A}$ denotes the set of generalized functions of the form

$$f(t) = \begin{cases} 0, & t < 0 \\ \sum_{i=0}^\infty f_i \delta(t - t_i) + f_a(t), & t \ge 0 \end{cases}$$

where $\delta(\cdot)$ is the unit delta distribution, t_i are non-negative constant delays, $f_a(t)$ is measurable and

$$\textstyle\sum_{i=0}^\infty |f_i| < \infty, \qquad \int_0^\infty |f_a(t)| dt < \infty.$$

Definition 5: $\hat{\mathcal{A}}$ denotes the set of all function $\hat{f} : \mathcal{C}_+ \to \mathcal{C}$ that are Laplace transforms of elements of $\mathcal{A}$.

A system is hence $\mathcal{L}_p$-stable if the internal signals are all integrable using the $\mathcal{L}_p$-norm, given external exciting signals that are also in $\mathcal{L}_p$, for some p.

The Nyquist and Popov criteria can now be formulated:

Lemma 1 (Nyquist Criterion, [26] Theorem 6.6.58): Consider the system of Fig. 3 with the static nonlinearity replaced by $\varphi(\sigma) = k\sigma$. Assume that the inverse Laplace transform of the transfer function $\hat{g}(s)$ fulfils $g(\cdot) \in \mathcal{A}$. Then the system is $\mathcal{L}_2$-stable if and only if the Nyquist plot

$$\omega \in [0, \infty) \to Re[\hat{g}(j\omega)] + jIm[\hat{g}(j\omega)] \in \mathcal{C}$$

is bounded away from and does not encircle $-\frac{1}{k} + j0$.

Proof: See [26], section 6.6.

Lemma 2 (Popov Criterion, [26] Theorem 6.7.63): Consider the system of Fig. 3. Assume that the inverse Laplace transform of the transfer function $\hat{g}(s)$ fulfils

$$g(\cdot) \in \mathcal{A}, \qquad \dot{g}(\cdot) \in \mathcal{A},$$

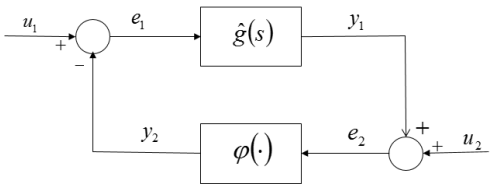

Fig. 3. Block diagram of [26] for which Lemma 1 and Lemma 2 are formulated. The loop gain, the static nonlinearity and the signals are scalar quantities. There are two inputs u_1 and u_2 but no output from the loop. The reason is that it is the output *feedback* that affects the stability and not the outputs as such. Therefore, if so desired, any of the internal signals y_1 and y_2 can be defined as outputs drawn as arrows leaving the loop.

that the time invariant static nonlinearity $\varphi(\cdot)$ fulfils

$$0 \le \sigma\varphi(\sigma) \le k\sigma^2,$$

and that $u_1 \in \mathcal{L}_2$, $u_2 \in \mathcal{L}_2$, $\dot{u_2} \in \mathcal{L}_2$. Under these conditions the system is $\mathcal{L}_2$-stable if there exist constants q, δ, such that the Popov plot

$$\omega \in [0, \infty) \to Re[\hat{g}(j\omega)] + j\omega Im[\hat{g}(j\omega)] \in \mathcal{C}$$

is entirely to the right of a line through $-1/k + \delta + j0$ with slope $1/q$, for some $q \ge 0$ and some $\delta > 0$.

Proof: See [26], section 6.7.

Note that no assumptions on u_1 and u_2 are listed in Lemma 1, since these are implicit from Definition 3. Furthermore, the Nyquist criterion is formulated for a stable loop gain. Note also that the geometrical condition on the Popov plot can be interpreted as the following inequality

$$Re[(1 + j\omega q)\hat{g}(j\omega)] + \frac{1}{k} \ge \delta > 0, \ \forall \omega \ge 0, \ q > 0. \quad (21)$$

B. External Signal Properties

Referring to Fig. 3, the stability of the delay skew control system can be analyzed once the loop gain of the delay skew control loop from $x_1(s)$ to $e_{skew}(s)$ and its properties are known. This means that the dynamics of the parts of Fig. 2 associated with the delay sum signal need to be eliminated, and that $T_{skew}^{ref}(s)$ and $T_{sum}^{ref}(s)$ become external signals. The delay signals $T_1^{DL}(s)$ and $T_2^{DL}(s)$ are also treated as external signals, with the corresponding fixed nominal quantities T_1^{DL} and T_2^{DL} approximating the delay effects represented by complex exponentials in (13)-(20). This approximate treatment is necessary to enable the analysis below.

An additional problem associated with the theory occurs in case an external signal has a non-zero bias. This bias will then e.g. become a part of the external signal u_2 of the Popov criterion, when the delay skew control system of Fig. 2 is transformed into the block diagram of Fig. 3 in the next section. This would invalidate the integrability conditions of the Popov criterion that require u_1 and u_2 to be in $\mathcal{L}_2$. One solution to the problem is to apply a change of variables, to change the signal levels so that all bias is removed. The static nonlinearity would then need to be changed accordingly.

Another alternative that is used here is to define external signals, with the following modified model of the bias

$$|f_{bias}(t)| \leq \begin{cases} |f_{bias,0}|, & 0 \leq t \leq T_{bias,break} \\ |f_{bias,0}| \frac{T_{bias,break}^{\frac{1}{2}+\gamma}}{t^{\frac{1}{2}+\gamma}}, & t > T_{bias,break}. \end{cases} \tag{22}$$

Here $f_{bias,0}$ denotes the bias component of the external signal and T_{break} is the time where a very slow decay begins. The signal $f_{bias}(t)$ now meets the $\mathcal{L}_2$ integrability condition since $\gamma > 0$, and both Lemma 1 and Lemma 2 become applicable. The decay is much slower than the exponential decay of an exponentially stable or asymptotically stable linearly generated signal. At the same time the selection of decay in (21) would allow exponential instability or limit cycles to be detected e.g. in a numerical simulation.

C. Assumptions

In addition to A1 - A4, the following assumptions on the delay skew control system are now needed

- A5) The inner loop transfer functions $G_i^{inner}(s)$, $i = 1, ..., 2$ are strictly proper.
- A6) The inner loops are $\mathcal{L}_2$-stable.
- A7) $T_{skew}^{ref} \in \mathcal{L}_2$ and $\dot{T}_{skew}^{ref} \in \mathcal{L}_2$.
- A8) $T_{sum}^{ref} \in \mathcal{L}_2$.
- A9) $T_i^{DL} \in \mathcal{L}_2$ and $\dot{T}_i^{DL} \in \mathcal{L}_2$, $i = 1, 2$.
- A10) $C_{skew}(s)$ and $C_{sum}(s)$ are proper.

The assumption A5 is e.g. valid for the inner loop controllers of [27]-[30]. To show this it is noted that the plant of the inner loop is the leaky queue $(s+\varepsilon)^{-1}$, where ε is the adaptive queue management (AQM) packet discard rate, see [25] and [27]. Since the lead lag controller of [27] is proper with 2 poles and 2 zeros, straightforward calculations show that (8) has three poles and two zeros in addition to the delay dynamics and A5 holds. The state space controllers of [28]-[30] do not have a direct term and are therefore strictly proper. Straightforward calculations then show that also (9) is strictly proper, and A5 holds in case of state space control as well. The controllers of [27]-[30] are designed to be $\mathcal{L}_2$-stable by pre-computation of the stability region, therefore A6 is a reasonable assumption. The assumptions on the external signals in A7-A9 are needed to comply with the conditions of Lemma 1 and Lemma 2. The conditions mean that the signals have a sufficient high frequency roll-off, which is needed for suppression of any high frequency components in the loop of Fig. 3 that could otherwise lead to instability. The assumptions on the controller filters in A10 are e.g. met by lead-lag controllers and by state space controllers like those of [28]-[30], also with a direct term added. In addition to A5-A10, the outer delay skew control loop gain needs to be internally $\mathcal{L}_2$-stable. Rather than introducing this as a condition, the Nyquist condition of Lemma 1 is included as a condition in the main result.

D. Loop Transformations and Stability

In order to prove that the Popov criterion of Lemma 2 is applicable to a stability analysis of the delay skew control system, the block diagram of Fig. 2 needs to be transformed to the block diagram of Fig. 3. The first step is then to compute $x_2(s)$. Using (2) in combination with the second row of (12) results in

$$\begin{aligned} x_2(s) = T_{sum}^{ref}(s) - A_{21}(s)x_1(s) - A_{22}(s)x_2(s) \\ -B_{21}(s)T_1^{DL}(s) - B_{22}(s)T_2^{DL}(s), \end{aligned} \tag{23}$$

which gives

$$\begin{aligned} x_2(s) = \frac{1}{1+A_{22}(s)}T_{sum}^{ref}(s) - \frac{A_{21}(s)}{1+A_{22}(s)}x_1(s) \\ -\frac{B_{21}(s)}{1+A_{22}(s)}T_1^{DL}(s) - \frac{B_{22}(s)}{1+A_{22}(s)}T_2^{DL}(s). \end{aligned} \tag{24}$$

Next, using (1) together with the first row of (12), and inserting (24) results in the relation

$$\begin{aligned} e_{skew}(s) = -\left(A_{11}(s) - \frac{A_{12}(s)A_{21}(s)}{1+A_{22}(s)}\right)x_1(s) \\ +T_{skew}^{ref}(s) - \frac{A_{12}(s)}{1+A_{22}(s)}T_{sum}^{ref}(s) \\ +\left(\frac{A_{12}(s)B_{21}(s)}{1+A_{22}(s)} - B_{11}(s)\right)T_1^{DL}(s) \\ +\left(\frac{A_{12}(s)B_{22}(s)}{1+A_{22}(s)} - B_{12}(s)\right)T_2^{DL}(s). \end{aligned} \tag{25}$$

A joint consideration of Fig. 2 and Fig. 3, then shows that

$$\begin{aligned} e_2(s) = \hat{g}(s)e_1(s) + u_2(s) = \hat{g}(s)(u_1(s) - y_2(s)) + u_2(s) \\ = -\hat{g}(s)x_1(s) + \hat{g}(s)u_1(s) + u_2(s). \end{aligned} \tag{26}$$

Finally, a comparison between (25) and (26) shows that

$$\hat{g}(s) = A_{11}(s) - \frac{A_{12}(s)A_{21}(s)}{1+A_{22}(s)}, \tag{27}$$

$$u_1(s) = 0, \tag{28}$$

$$\begin{aligned} u_2(s) = T_{skew}^{ref}(s) - \frac{A_{12}(s)}{1+A_{22}(s)}T_{sum}^{ref}(s) \\ +\left(\frac{A_{12}(s)B_{21}(s)}{1+A_{22}(s)} - B_{11}(s)\right)T_1^{DL}(s) \\ +\left(\frac{A_{12}(s)B_{22}(s)}{1+A_{22}(s)} - B_{12}(s)\right)T_2^{DL}(s). \end{aligned} \tag{29}$$

To conclude on the applicability of Lemma 2, the properties of (27)-(29) are analyzed based on A1-A10, with the purpose of showing that the signal and loop gain conditions of Lemma 2 are implied. As a side effect the conditions of Lemma 1 follow from this discussion. It is first noted that A1-A4 imply that the inner loops may be treated as linear transfer functions given by (8) or (9), with non-negative inputs. It then follows by A5, A10 and (13)-(16) that $A_{11}(s)$, $A_{12}(s)$, $A_{21}(s)$ and $A_{22}(s)$ are strictly proper. In the same way it follows that $B_{11}(s)$, $B_{12}(s)$, $B_{21}(s)$ and $B_{22}(s)$ are proper, by A5 and (17)-(20). $B_{11}(s)$, $B_{12}(s)$, $B_{21}(s)$ and $B_{22}(s)$ are not necessarily strictly proper, unless the static gains of the inner loops are exactly

equal to 1. In addition, assumption A6 immediately implies that $A_{11}(s)$, $A_{12}(s)$, $A_{21}(s)$, $A_{22}(s)$, $B_{11}(s)$, $B_{12}(s)$, $B_{21}(s)$ and $B_{22}(s)$ are $\mathcal{L}_2$-stable.

A straightforward evaluation of (27) using the results above shows that the loop gain of (27) given by $A_{11}(s) - A_{12}(s)\left(1+A_{22}(s)\right)^{-1}A_{21}(s)$ is strictly proper. It remains to establish $\mathcal{L}_2$-stability of $A_{11}(s) - A_{12}(s)\left(1+A_{22}(s)\right)^{-1}A_{21}(s)$. It was shown above that $A_{11}(s)$, $A_{12}(s)$, $A_{21}(s)$ and $A_{22}(s)$ are all $\mathcal{L}_2$-stable. It hence remains to prove that also $\left(1+A_{22}(s)\right)^{-1}$ is $\mathcal{L}_2$-stable. This can be done by means of Lemma 1 by noting that the choice of $\varphi(\sigma)=\sigma$ and $\hat{g}(s)=A_{22}(s)$ in Lemma 1 imply the following relation, referring to Fig. 3

$$y_1(s) = \frac{A_{22}(s)}{1+A_{22}(s)}\left(u_1(s)-u_2(s)\right). \tag{30}$$

If the Nyquist criterion of Lemma 1 holds for the loop gain $A_{22}(s)$, it therefore follows that $\left(1+A_{22}(s)\right)^{-1}$ is $\mathcal{L}_2$-stable. This Nyquist condition on $A_{22}(s)$ is included in the formulation of Theorem 1 below. This assumption involving the Nyquist condition now implies that $\hat{g}(s)$ of (27) is $\mathcal{L}_2$-stable, and it follows from [26], Theorem 6.5.37, that $g(\cdot)\in\mathcal{A}$ and that $\dot{g}(\cdot)\in\mathcal{A}$. This proves the first requirement of Lemma 2.

The condition that $u_1\in\mathcal{L}_2$ immediately follows from (28).

The remaining condition of Lemma 2 is that $u_2\in\mathcal{L}_2$ and that $\dot{u}_2\in\mathcal{L}_2$. To evaluate this condition, the terms of (29) are considered. First A7 implies that T_{skew}^{ref} meets the condition on the signal u_2. The second term of (29) is composed of $T_{sum}^{ref}\in\mathcal{L}_2$ filtered by $A_{12}(s)\left(1+A_{22}(s)\right)^{-1}$. Since $A_{12}(s)$ and $A_{22}(s)$ are strictly proper, $A_{12}(s)\left(1+A_{22}(s)\right)^{-1}$ is also strictly proper. By using the discussion above and the Nyquist condition, the filter is also $\mathcal{L}_2$-stable. Therefore, by A8, the second term and its derivative are both in $\mathcal{L}_2$. The third term is composed of $T_1^{DL}(s)$ filtered by the transfer function $A_{12}(s)B_{21}(s)\left(1+A_{22}(s)\right)^{-1}-B_{11}(s)$ which is at least proper and $\mathcal{L}_2$-stable, following the previous discussion. By A9, it therefore follows that the third term and its derivative are both in $\mathcal{L}_2$. The fourth term and its derivative are in $\mathcal{L}_2$ by an identical argumentation. Since $\mathcal{L}_2$ is a linear space it follows that $u_2\in\mathcal{L}_2$ and that $\dot{u}_2\in\mathcal{L}_2$.

Finally, noting that the static nonlinearity (3) meets the sector condition $0\le\sigma\varphi(\sigma)\le 1\sigma^2$, the following result has been proved:

Theorem 1: Consider the delay skew control system of Fig. 2 with delay skew control loop gain

$$\hat{g}(s) = A_{11}(s) - \frac{A_{12}(s)A_{21}(s)}{1+A_{22}(s)}$$

defined by (8), (9), (13)-(20), and assume that A1-A10 hold. Then, if the deadzone fulfils

$$0\le\sigma\varphi(\sigma)\le 1\sigma^2$$

and if the Nyquist plot of $A_{22}(s)$

$$\omega\in[0,\infty)\rightarrow Re[A_{22}(j\omega)]+jIm[A_{22}(j\omega)]\in\mathcal{C}$$

is bounded away from and does not encircle $-1+j0$, then the delay skew control system is $\mathcal{L}_2$-stable if there exists constants q, δ, such that the Popov plot of the delay skew control loop gain given by

$$\omega\in[0,\infty)\rightarrow Re[\hat{g}(j\omega)]+j\omega Im[\hat{g}(j\omega)]\in\mathcal{C}$$

is entirely to the right of a line through $-1+\delta+j0$ with slope $1/q$, for some $q\ge 0$ and some $\delta>0$.

Note again that the Nyquist condition has been included in Theorem 1 since it represents a graphical stability criterion that needs to be evaluated in addition to the Popov criterion, for Theorem 1 to hold. The Nyquist condition ensures the internal stability of the delay skew control loop gain. Note also that all delays are embedded in the transfer functions of (13)-(20). This is possible since Lemma 1 and Lemma 2 are valid for infinite dimensional systems.

IV. Reference Tracking and Disturbance Rejection

A. Linear Closed Loop Model

The present section specializes to the linear delay skew control case by the assumption

A11) The deadzone $\Delta T_{skew}=0.0$.

Because of A11 it holds that

$$\begin{pmatrix} x_1(s)\\ x_2(s)\end{pmatrix} = \begin{pmatrix} T_{skew}^{ref}(s)\\ T_{sum}^{ref}(s)\end{pmatrix} - \begin{pmatrix} T_{skew}(s)\\ T_{sum}(s)\end{pmatrix}. \tag{31}$$

Insertion of (31) in (12) and a re-arrangement gives the equation

$$\begin{pmatrix} T_{skew}(s)\\ T_{sum}(s)\end{pmatrix} = \left(\mathbf{I}+\mathbf{A}(s)\right)^{-1}\mathbf{A}(s)\begin{pmatrix} T_{skew}^{ref}(s)\\ T_{sum}^{ref}(s)\end{pmatrix} + \left(\mathbf{I}+\mathbf{A}(s)\right)^{-1}\mathbf{B}(s)\begin{pmatrix} T_1^{DL}(s)\\ T_2^{DL}(s)\end{pmatrix}, \tag{32}$$

where $\mathbf{I}$ denotes the second order identity matrix. The relation (32) is the counterpart to the conventional single-input-single-output (SISO) reference tracking and disturbance rejection model.

B. Static Properties

Assume that reference and disturbance step signals are applied to the system, according to

$$\begin{pmatrix} T_{skew}^{ref}(s)\\ T_{sum}^{ref}(s)\end{pmatrix} = \frac{1}{s}\begin{pmatrix} \bar{T}_{skew}^{ref}\\ \bar{T}_{sum}^{ref}\end{pmatrix}, \tag{33}$$

$$\begin{pmatrix} T_1^{DL}(s)\\ T_2^{DL}(s)\end{pmatrix} = \frac{1}{s}\begin{pmatrix} \bar{T}_1^{DL}\\ \bar{T}_2^{DL}\end{pmatrix}. \tag{34}$$

Since A1-A11 hold, the closed loop system (32) is $\mathcal{L}_2$-stable. The static properties of (32) therefore follow immediately from an application of the standard final value theorem [26] using (33) and (34) to achieve

$$\lim_{t\rightarrow\infty}\begin{pmatrix} T_{skew}(t)\\ T_{sum}(t)\end{pmatrix} = \lim_{s\rightarrow 0} s\begin{pmatrix} T_{skew}(s)\\ T_{sum}(s)\end{pmatrix}$$

$$\left(\mathbf{I}+\mathbf{A}(0)\right)^{-1}\mathbf{A}(0)\begin{pmatrix} \bar{T}_{skew}^{ref}\\ \bar{T}_{sum}^{ref}\end{pmatrix}$$

$$+\left(\mathbf{I}+\mathbf{A}(0)\right)^{-1}\mathbf{B}(0)\begin{pmatrix}\bar{T}_1^{DL}\\ \bar{T}_2^{DL}\end{pmatrix}. \quad (35)$$

This equation can be used to enhance the understanding of the delay skew controller in the case where the inner loop properties and backhaul delays are uncertain and differ significantly. In such a case it is clear the if $\|\mathbf{A}(0)\|$ is large, then the reference tracking will be good at the same time as the rejection of the downlink delay disturbance $\begin{pmatrix}\bar{T}_1^{DL} & \bar{T}_2^{DL}\end{pmatrix}^T$ will be good. This follows from (13) - (20) that show that $\|\mathbf{A}(0)\|$ can be made large by selecting large values of $C_{skew}(0)$ and $C_{sum}(0)$, without affecting $\|\mathbf{B}(0)\|$. However, this approach may become infeasible when the delay skew loop delay becomes significant. The reason is that the low frequency loop gain needs to stay below a quantity determined by its poles and zeros when the loop delay tends to infinity, as proved by Theorem 2 of [29]. This low frequency limitation makes it interesting to study the reference tracking and disturbance rejection properties in further detail.

C. Dynamic Reference Tracking and Disturbance Rejection

Introduce the following assumptions:

A12) $\hat{g}_1(s)=\hat{g}_2(s)$.
A13) $|T_1^{DL}-T_2^{DL}|\to 0$.
A14) $|T_1^{UL}-T_2^{UL}|\to 0$.

where the conditions on the delays are valid for nominal fixed delays. It then follows from (8), (9), A12, A13 and A14 that the inner loops fulfil $G_1^{inner}(s)=G_2^{inner}(s)$. When A14 is assumed to hold the implication of (14) and (15) is that $A_{12}(s)=A_{21}(s)=0$, i.e. $\mathbf{A}(s)$ becomes diagonal. When this fact is applied to (32), it simplifies to the following result:

Theorem 2: Assume that A1-A14 hold. Then

$$T_{skew}(s)\to\frac{C_{skew}(s)G_1^{inner}(s)e^{-sT_1^{UL}}}{1+C_{skew}(s)G_1^{inner}(s)e^{-sT_1^{UL}}}T_{skew}^{ref}(s)$$

$$+\frac{\left(1-G_1^{inner}(s)\right)e^{-sT_1^{UL}}}{1+C_{skew}(s)G_1^{inner}(s)e^{-sT_1^{UL}}}\left(T_1^{DL}(s)-T_2^{DL}(s)\right).$$

$$T_{sum}(s)\to\frac{C_{sum}(s)G_2^{inner}(s)e^{-sT_2^{UL}}}{1+C_{sum}(s)G_2^{inner}(s)e^{-sT_2^{UL}}}T_{sum}^{ref}(s)$$

$$+\frac{\left(1-G_2^{inner}(s)\right)e^{-sT_2^{UL}}}{1+C_{sum}(s)G_2^{inner}(s)e^{-sT_2^{UL}}}\left(T_1^{DL}(s)+T_2^{DL}(s)\right).$$

The conclusion of Theorem 2 is that the conditions A12-A14 imply that reference tracking decoupling between the delay sum and delay skew channels is achieved. However, disturbance rejection is not necessarily achieved.

The following additional assumption is needed to address also the disturbance rejection performance.

A15) $|G_i^{inner}(j\omega)-1|<\delta$, $\delta>0$, $i=1,2$, when $\omega<\omega_{outer}$.

Here ω_{outer} represents the bandwidth of the outer delay skew control loop. The assumption A15 gives in the following result that bounds the second terms of $T_{skew}(s)$ and $T_{sum}(s)$:

Corollary 1: Consider the delay skew control system of Fig. 2 and assume that A1-A15 hold. Then also disturbance rejection is achieved in the sense that for $\omega\le\omega_{outer}$

$$\left|\frac{\left(1-G_1^{inner}(j\omega)\right)e^{-j\omega T_1^{UL}}}{1+C_{skew}(j\omega)G_1^{inner}(j\omega)e^{-j\omega T_1^{UL}}}\left(T_1^{DL}(j\omega)-T_2^{DL}(j\omega)\right)\right|$$

$$\le\delta K_1|T_1^{DL}(j\omega)-T_2^{DL}(j\omega)|,$$

$$\left|\frac{\left(1-G_2^{inner}(j\omega)\right)e^{-j\omega T_2^{UL}}}{1+C_{sum}(j\omega)G_2^{inner}(j\omega)e^{-j\omega T_2^{UL}}}\left(T_1^{DL}(j\omega)+T_2^{DL}(j\omega)\right)\right|$$

$$\le\delta K_2|T_1^{DL}(j\omega)+T_2^{DL}(j\omega)|.$$

Above, $K_1<\infty$ and $K_2<\infty$ are constants formed from the denominators of the transfer functions, using the fact that the system dynamics is $\mathcal{L}_2$-stable. There are therefore no singularities on the imaginary axis.

In summary, it could be concluded that a good inner loop controller design is essential if good disturbance rejection shall be achieved. In addition, a system design with similar inner control loop dynamics is beneficial in terms of decoupling between the transmission node paths.

V. Numerical Results

This section evaluates the performance of the proposed delay skew controller using prototype test code, applied to test data generated in 4G system simulations. This is believed to give a good prediction also of the 5G performance since the delays and sampling period are selected to be close to 1 ms, and since the radio access methods of 4G and 5G both use orthogonal frequency division multiple access (OFDMA) [3].

A. Detailed Delay Skew Controller Design

The delay skew NCS is designed for backhaul delays that are typically less than 5 ms, but that may increase to $T_i^{DL}=T_i^{UL}=20$ ms, $i=1,2$, occasionally. The delay skew NCS should remain stable for these delays.

The delay skew controller design procedure starts with the design of the two inner loops. The guidance provided by Theorem 2 and Corollary 1 suggests that the NCS should be designed with symmetric inner loops, with a bandwidth high enough to appear ideal as seen by the outer delay skew control loop. The two inner loop controllers were therefore designed to be identical. The control objective includes a requirement on the transmit data queues, stating that they should not cause data starvation or an unnecessarily high dwell time. The data flow controller of [27] was therefore selected since it is based on dwell time feedback control. That controller consists of a lead-lag feedback link acting together with a feedforward filter, thereby combining queue dwell time feedback with wireless rate feedforward. The feedforward filter does neither affect the stability of the delay skew NCS, nor the outer delay skew control loop design and it is therefore not discussed in detail. In summary, the feedforward control signal is obtained as

$$u_{FF}(s)=\frac{\omega_0^2}{s^2+2\xi_0\omega_0 s+\omega_0^2}w(s), \quad (36)$$

where $w(s)$ denotes the air interface rate. The numerical values are $\xi_0 = 1.0$ and $\omega_0 = 4190\ rad/s$. The bandwidth is much higher than the feedback bandwidth and it was selected with experiments using the testbed.

The lead-lag feedback link transfer function is given by

$$C_i^{inner}(s) = K\frac{s+a}{s+\frac{a}{M}}N\frac{s+b}{s+Nb}, \quad i = 1, 2, \qquad (37)$$

where the parameters are discussed below. Together with the queue dynamics s^{-1}, this results in the loop gain

$$\hat{g}_i(s) = K\frac{s+a}{s+\frac{a}{M}}N\frac{s+b}{s+Nb}\frac{1}{s}, \quad i = 1, 2. \qquad (38)$$

Note that (38) is here defined without the loop delay, to be consistent with the notation of (8) and (9).

The design of the lead-lag link is described in [27], the reader is referred to that publication for the mathematical details. Briefly, the design procedure is as follows. First the desired bandwidth is specified in terms of a cross-over frequency where the absolute value of the loop gain equals 1, accounting for the queue dynamics and the loop delay. The desired stability properties are determined by the phase margin, at the cross-over frequency. The results reported in the present paper are based on a cross-over frequency of $f_c = 7.33\ Hz$ and a phase margin of $\varphi_m = 55.0\ deg$. Note that angular cross-over frequency becomes $\omega_c = 2\pi f_c = 46\ rad/s \approx 1/0.025\ rad/s$ which means that the selection is consistent with the expected maximum loop delays, assuming independence between the uplink and the downlink. This selection secures stability, cf. [29]. In order to determine the phase advance needed by the lead filter $(s+b)/(s+Nb)$, the phase of the other factors of the loop gain (38) needs to be known, hence the parameters a and M need to be determined first. M determines the amount of low frequency gain since the static gain of the lag filter $(s+a)/(s+a/M)$ is M. To allow good regulation of stationary errors $M = 10.0$ is selected, to give 20 dB of additional low frequency gain. The parameter a influences the transient properties of the controller. Testbed experiments resulted in the selection $a = 0.05 \times 2\pi f_c = 2.30\ rad/s$. The phase at the cross over frequency of all factors of (38) except the lead filter, together with the loop delay phase contribution, are then available. To meet the phase margin, the lead filter needs to provide 23.0 deg of additional phase advance which results in the parameters $b = 30.49\ rad/s$ and $N = 2.28$, cf. [27]. Finally K is determined from the condition that the loop gain shall equal 1, i.e $|\hat{g}_i(j2\pi f_c)| = 1$. This gives $K = 30.45\ rad/s$ and the controller filter

$$C_i^{inner}(s) = 69.43\frac{(s+2.30)}{(s+0.23)}\frac{(s+30.49)}{(s+69.51)}, \quad i = 1, 2. \qquad (39)$$

The Bode plot of the resulting inner loop transfer function (8) appears in Fig. 4.

The next step is to design the outer delay skew and delay sum controller filters. Also these filters are designed to be the same. Since cascade control is applied, these filters should result in a lower bandwidth than the corresponding inner loops. Here $C_{sum}(s)$ and $C_{skew}(s)$ are designed to give a bandwidth that is half that of the inner loops. Also $C_{skew}(s)$ and $C_{sum}(s)$

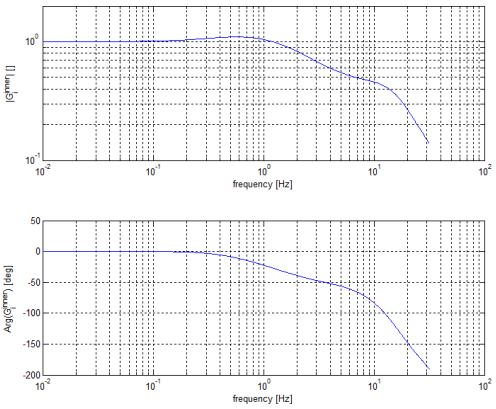

Fig. 4. Bode plot of the lead lag inner feedback loops for the assumed delays. The cross-over frequency was set to 7.3 Hz.

were selected as lead-lag controllers, determined from the inner loop dynamics of (8) multiplied with the uplink delay dynamics $e^{-sT_i^{UL}}$, $i = 1, 2$. In this case no phase advance is needed, although a phase margin of $\varphi_m = 75.0\ deg$ is specified, hence no lead filter is needed. Testbed experiments were then used to arrive at the lag filter parameters $M = 10$ and $a = 0.25 \times 0.5 \times 2\pi\ f_c = 5.76\ rad/s$. This gave $K = 1.56$ and the filters are

$$C_{skew}(s) = C_{sum}(s) = 1.56\frac{s+5.76}{s+0.57}. \qquad (40)$$

All controller filters were then discretized using Tustin's approximation [19], [27]. This second order approximation is given by the replacement

$$s \rightarrow \frac{2}{T_s}\frac{1-q_{T_s}^{-1}}{1+q_{T_s}^{-1}}. \qquad (41)$$

Here the sampling period is $T_s = 3.0\ ms$ and $q_{T_s}^{-1}$ denotes the time shift operator. This completes the controller design.

B. $\mathcal{L}_2$-stability

As stated above a key performance requirement is that the delay skew NCS should be stable for loop delays up to at least $T_i^{DL} + T_i^{UL} = 25\ ms$, assuming that the downlink and uplink do not experience the maximum delay simultaneously. To assess this robustness property, T_1^{DL} was varied for $T_2^{UL} = T_i^{UL} = 2.0\ ms$, $i = 1, 2$. The controller filter parameters were as computed in the previous subsection, with $G_i^{inner}(s)$ and the components of $\mathbf{A}(s)$ of (8) and (12) varying with T_1^{DL}. This variation is the same as in the performance evaluation below.

To assess the $\mathcal{L}_2$-stability of the delay skew NCS, Theorem 1 was applied. The conditions A1-A10 were all found reasonable in the discussion of section III.C. Noting that all of the designed controller filters are stable and proper, Theorem 1 is therefore valid. The Nyquist and Popov plots that define stability were then computed for varying T_1^{DL}. This resulted in Fig. 5 and Fig. 6.

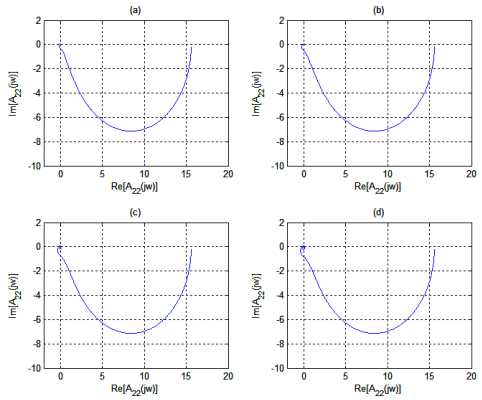

Fig. 5. Nyquist plots of $A_{22}(s)$ for $T_1^{DL} = 0.002\ s$ (a), $T_1^{DL} = 0.0125\ s$ (b), $T_1^{DL} = 0.025\ s$ (c), and $T_1^{DL} = 0.030\ s$ (d). $T_2^{DL} = T_i^{UL} = 0.002\ s,\ i = 1, 2$. Note that the convention in control is to plot only the part of the Nyquist curve that corresponds to positive frequencies. Since the negative frequencies appear mirrored in the real axis, cf. [26], this is easily exploited when interpreting the Nyquist plots.

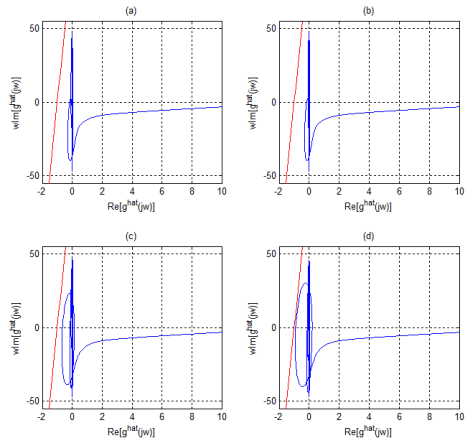

Fig. 6. Popov plots of $\hat{g}(s)$ using $q = 0.01$. $T_1^{DL} = 0.002\ s$ (a), $T_1^{DL} = 0.0125\ s$ (b), $T_1^{DL} = 0.025\ s$ (c), and $T_1^{DL} = 0.030\ s$ (d). $T_2^{DL} = T_i^{UL} = 0.002\ s,\ i = 1, 2$.

The Popov plots are the ones that limit stability. Applying Theorem 1, these plots show that the delay skew NCS is globally $\mathcal{L}_2$-stable at least for loop delays less than 30 ms. The stability requirements of the paper are therefore met.

C. Test Code Implementation

The delay skew controller was implemented in C++ . Following a conventional controller performance evaluation, the same code can then also be integrated and run on product hardware. This allows the computational complexity to be evaluated at multi-core DSP cycle level which is much more accurate than estimates obtained by counts of arithmetic operations. The code can also directly form the basis for product code development.

The testbed code implements the lead-lag queue dwell time inner loop controller of [27] which is used in the present paper. For the DC application two wireless transmission nodes are used. The tuning of the inner loop controllers can be parameterized either in terms of all the controller parameters, or in terms of a single parameter that represents the nominal round trip loop delay. All other controller parameters are then derived from the nominal round trip loop delay. One single user parameter is therefore enough to set the controller parameters, for nominal round trip loop delays from hundreds of ms down to a fraction of a ms. This is possible since the tuning of a lead-lag controller starts by definition of the crossover angular frequency [27]. Since an increased delay requires a reduced angular crossover frequency it holds that

$$\omega_c = \frac{C_{\omega_c}}{T_{RTT}^{nominal}}. \tag{42}$$

Here C_{ω_c} is a scale factor corresponding to a well working controller tuning. All lead-lag link parameters then follow from ω_c using the procedure of [27]. The delay skew and delay sum controller filters are selected to be lead-lag links, exactly as in [27]. Also these controller filters can be parameterized in terms of all controller parameters of the lead-lag link, or in terms of the nominal round trip loop delay.

The inner loop implementation embeds a simulation of each data transmission between the controller node and the wireless transmission nodes. The delays in the downlinks and uplinks can be varied independently to simulate time variation, using buffers to implement backhaul delays. The inner loop implementation also simulates the transmit data queue of each wireless transmission node, thereby connecting to the wireless interfaces and data rates that empty the transmit data queues. Any wireless simulator may be used for the generation of the wireless data rates, however the testbed code can also interface to external test files that provide the wireless data rate that affects each transmit data queue volume. In this way the inner loop simulation provides the time evolution of all delays of the loops. The inner loop controller simulation is capable of producing output data files readable by MATLAB, that are used for display of the obtained results. Input data rates to the controller node can be introduced with various traffic models, however this is beyond the scope of the present paper.

D. Performance

The performance of the algorithm was then assessed using the product testbed code. The delay sum control channel and the corresponding transmission node are denoted Tx point 0 in the results, while the delay skew control channel and the corresponding transmission node are denoted Tx point 1. The wireless bitrates were generated as the scheduled rates produced by a high fidelity system simulator using independent realizations of the typical urban channel model, with 3 $kmph$ movement. Examples of the wireless rate signals appear in Fig. 7

1) Delay skew control without deadzone: A case without deadzone is shown first, to illustrate the performance in an ideal case. The reference values were $T_{skew}^{ref} = 0.0\ ms$ and $T_{sum}^{ref} = 40\ ms$, respectively. This means that the total delay budget of 40 ms is to be distributed over the downlinks to achieve the delay skew control objective.

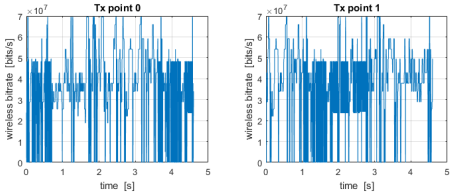

Fig. 7. The scheduled wireless rates.

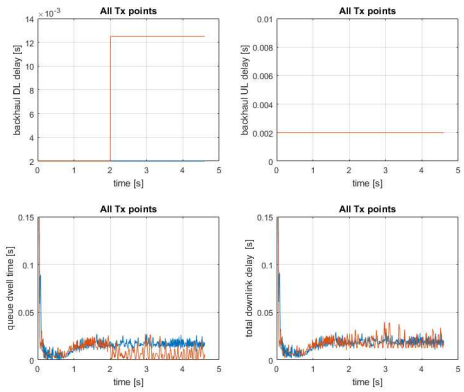

Fig. 8. Backhaul downlink delays, backhaul uplink delays, queue dwell times, and the total downlink delays.

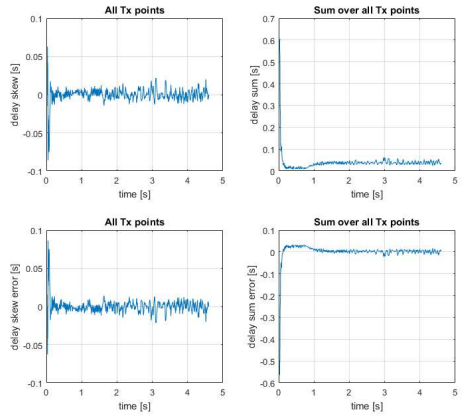

Fig. 9. Delay skew, delay sum and the corresponding errors.

The variation of the downlink and uplink backhaul delays for this case appears in Fig. 8. That figure also shows the resulting transmit data queue delays and the total downlink delays. During the first 2 s of the test it can be seen that the queue delays both converge to values just below 20 ms which reflects that the downlink delays are both 2 ms. The total downlink delay of both channels converge to about 20 ms. After 2 s of simulation Tx point 1 experiences a backhaul downlink delay of 12.5 ms. The delay skew controller responds by an immediate reduction of the corresponding queue delay to keep the total downlink delay at 20 ms. It can be seen that the control loop of Tx point 1 is less stable than that of Tx point 0, after 2 s. The reason is the higher downlink backhaul delay

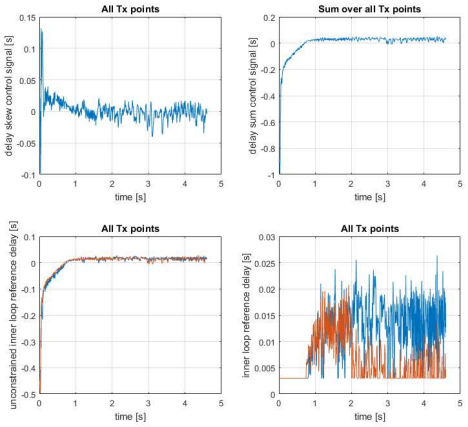

Fig. 10. The delay skew control signal $u_{skew}(t)$, the delay sum control signal $u_{sum}(t)$, the unconstrained inner loop reference delays as well as the (constrained) inner loop reference delays.

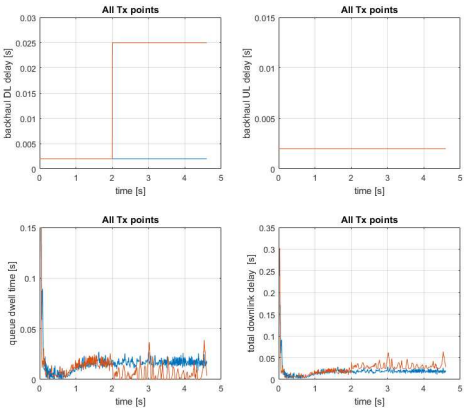

Fig. 11. Backhaul downlink delays, backhaul uplink delays, queue dwell times, and the total downlink delays.

corresponding to Tx point 1 at the end of the simulation. It can be seen in Fig. 8 that the delay skew controller distributes the total downlink delay budget equally between the two Tx points. This is the way T_{skew}^{ref} is achieved, something that is also illustrated by Fig. 9. The right plots of that figure also shows that also T_{sum}^{ref} is met. The various control signals that achieve this are depicted in Fig. 10. Note that the dwell time reference signals are not allowed to be lower than 3 ms.

2) Delay skew control with deadzone: Next, the effect of the deadzone is treated numerically. In order to do so, the backhaul downlink delay of Tx point 1 is increased as depicted in Fig. 11. The effect of the change is that T_{skew}^{ref} and T_{sum}^{ref} become inconsistent since there is no way to control the delay skew to zero, without increasing the total downlink delay of both Tx points to at least 25 ms, and the consequence would then be a zero transmit data queue delay which is not desirable. The result of the inconsistency can be seen in Fig. 11 and Fig. 12. The delay skew controller then fails to meet both T_{skew}^{ref} and T_{sum}^{ref} by compromising on both controlled quantities. That seems reasonable, however there is another

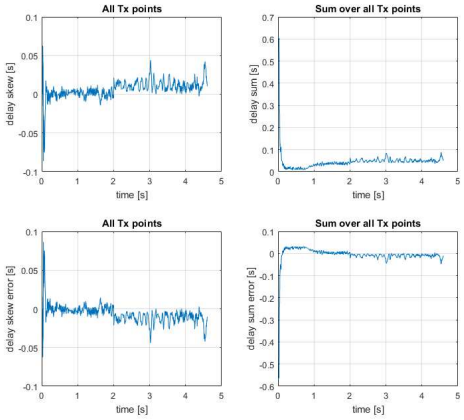

Fig. 12. Delay skew, delay sum and the corresponding errors.

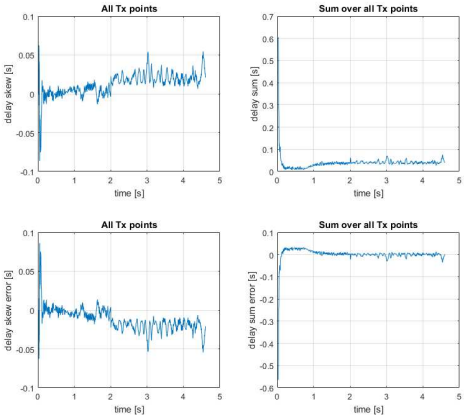

Fig. 14. Delay skew, delay sum and the corresponding errors.

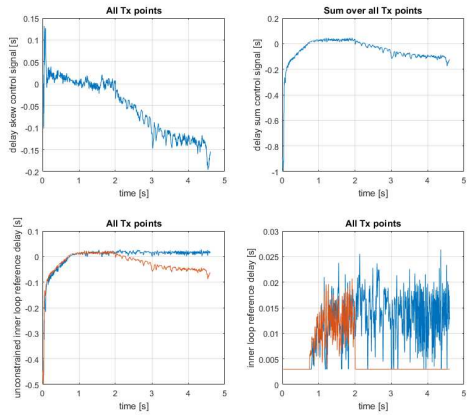

Fig. 13. The delay skew control signal $u_{skew}(t)$, the delay sum control signal $u_{sum}(t)$, the unconstrained inner loop reference delays as well as the (constrained) inner loop reference delays.

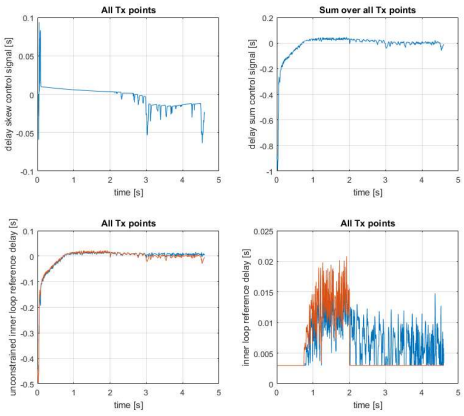

Fig. 15. The delay skew control signal $u_{skew}(t)$, the delay sum control signal $u_{sum}(t)$, the unconstrained inner loop reference delays as well as the (constrained) inner loop reference delays.

very undesirable effect. As seen in Fig. 13 the unconstrained inner loop reference delay signal for the inner loop of Tx point 1 becomes very negative, a fact that may lead to transient effects when the downlink backhaul delay is reduced. The lower right plot of Fig. 13 shows this clearly, since the inner loop reference value for Tx point 1 settles at the minimum allowed level of 3 ms after 2 s of the test.

The introduction of a deadzone with $\Delta T_{skew} = 25\ ms$ mitigates the problem as is evident from Fig. 14 and Fig. 15. In particular Fig. 14 shows that the delay skew is kept within the tolerance set by the deadzone, at the same time as the delay sum now meets $T_{sum}^{ref} = 40\ ms$. Fig. 15 shows that this is achieved by a delay skew control signal that, because of the deadzone, varies much less and results in an unconstrained reference for Tx point 1 that is much less negative. The deadzone hence achieves a robust back-off in case of a backhaul downlink delay that creates an inconsistency with the total delay budget.

3) Delay skew control with inactive dead-zone: It remains to study if the deadzone has any obvious negative side effects. Therefore the deadzone was retained, while the backhaul downlink delay was reduced to the consistent values of Fig. 8. As can be checked in Fig. 16 and Fig. 17 the delay skew NCS manages to keep the delay skew well below the tolerance set by the deadzone, at the same time as T_{sum}^{ref} is met. The delay skew control signal is also more smooth than without a deadzone. Finally, Fig. 18 and Fig. 19 illustrate the inner loop operation for Tx points 0 and 1. Note the decrease of the queue dwell time at time 2 s, at the time the downlink backhaul delay increases to 12.5 ms. In summary, the deadzone is capable of producing a back-off in case of delay inconsistency. This allows a reduced delay budget (T_{sum}^{ref}) to be used, which in turn should lead to reduced loop delays and increased capacity during normal operation of the delay skew NCS.

VI. Conclusions

The paper developed, analyzed and characterized a new delay skew control algorithm, supporting dual connectivity downlink data transmission in 4G and 5G wireless networks. The evaluation shows that the algorithm succeeds in regulating the data flow so that data items that are originally adjacent in time but travel over different internet and wireless interfaces

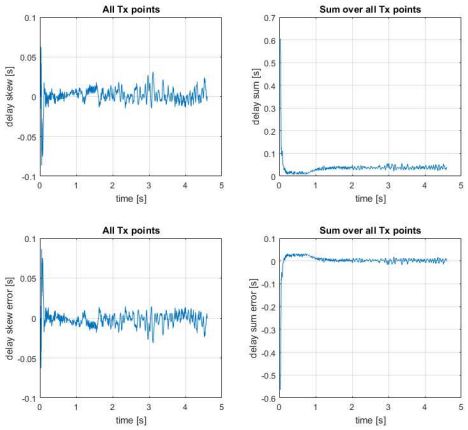

Fig. 16. Delay skew, delay sum and the corresponding errors.

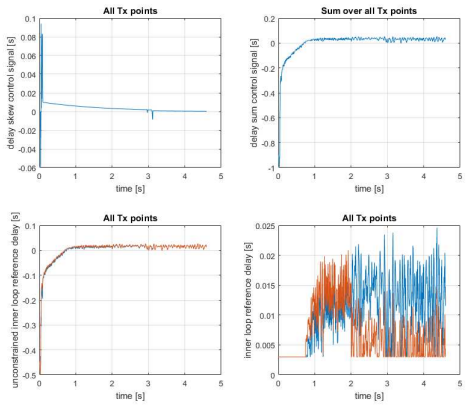

Fig. 17. The delay skew control signal $u_{skew}(t)$, the delay sum control signal $u_{sum}(t)$, the unconstrained inner loop reference delays as well as the (constrained) inner loop reference delays.

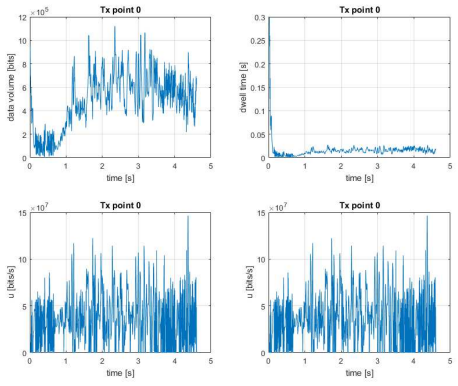

Fig. 18. Queue data volume, dwell time and control signal of Tx point 0.

also arrive at the mobile closely in time, despite significant differences and variations of the delays of the data paths and despite radio fading. This is important to maintain an efficient utilization of the air-interface resources and to maintain a stable data flow without re-ordering buffer resets. The

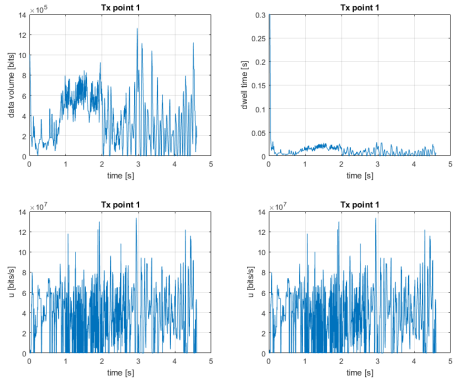

Fig. 19. Queue data volume, dwell time and control signal of Tx point 1.

proposed delay skew controller achieves the control objective with almost linear cascade control techniques, resulting in a low computational complexity which enables many parallel applications utilizing delay skew control in each node. In addition, the paper proves that the delay skew controller is globally input-output stable, provided that the data path delays are below a pre-computable limit. This conclusion is practically important since it guarantees that the flow control algorithms of the wireless system always operate as specified.

In addition, the paper concludes that good performance is related to high performing inner control loops, and to a symmetric design of the data paths and inner control loops. This information is useful e.g. when new wireless networks are deployed. The tuning of the control loops in the field is facilitated by the fact that the global input-output stability of the control system is quantified by the *graphical* frequency domain Nyquist- and Popov-criteria. The latter criterion addresses the deadzone of the controller that was found to enhance the operating region beyond that of a linear design.

There are many future research opportunities. An improved stability analysis to include a theoretical treatment of varying delays is one possibility. Furthermore, the new use cases discussed for 5G wireless systems have already lead to requirements on latency quality in a wide sense. This may lead to new optimization problems, where delay and capacity are jointly optimized for wireless transmission.

ACKNOWLEDGMENT

This research was supported under Australian Research Council's Linkage Projects funding scheme (project number LP150100757).

REFERENCES

[1] J. Baillieul and P. J. Antsaklis, "Control and communication challenges in networked real-time systems", *Proc. IEEE*, vol. 95, no. 1, pp. 9-28, 2007.

[2] N. Cardwell, Y. Cheng, C. S. Gunn, S. H. Yeganeh and V. Jacobson, "BBR congestion control", *Proc. IETF 97*, Seoul, South Korea, Nov. 2016. Available: https://www.ietf.org/proceedings/97/slides/slides-97-iccrg-bbr-congestion-control-02.pdf .

[3] E. Dahlman, S. Parkvall, J. Sköld and P. Beming, *3G Evolution - HSPA and LTE for Mobile Broadband.* Oxford, UK: Academic Press, 2008.

[4] R. Delgado, K. Lau, R. H. Middleton and T. Wigren, "Networked delay control for 5G wireless machine type communications using multi-connectivity", *submitted*, 2016.

[5] R. A. Delgado, T. Wigren, K. Lau and R. H. Middleton, "Stability properties of a MIMO data flow controller", *to appear in Proc. ACC* , Milwaukee, USA, June 27-29, 2018.

[6] Ericsson AB, "5G Radio Access - Research and Vision", *Ericsson White Paper 284 23-3204 Uen*, June, 2013. Available: http://www.ericsson.com/res/docs/whitepapers/wp-5g.pdf.

[7] Evolved Universal Terrestrial Radio Access (E-UTRA); Medium Access Control (MAC) protocol specification, July 2015, 3GPP TS 36.321, release 12 (v. 12.6.0). [Online]. Available: http://www.3gpp.org/DynaReport/36321.htm

[8] Universal Terrestrial Radio Access (E-UTRA); LTE physical layer; General description, March 2015, 3GPP TS 36.201, release 12 (v. 12.2.0). [Online]. Available: http://www.3gpp.org/DynaReport/36201.htm

[9] Evolved Universal Terrestrial Radio Access (E-UTRA); Packet Data Convergence Protocol (PDCP) specification, March 2015, 3GPP TS 36.323, release 12 (v. 12.3.0). [Online]. Available: http://www.3gpp.org/DynaReport/36323.htm

[10] Evolved Universal Terrestrial Radio Access (E-UTRA); Radio Link Control (RLC) protocol specification, March 2015, 3GPP TS 36.321, release 12 (v. 12.2.0). [Online]. Available: http://www.3gpp.org/DynaReport/36322.htm

[11] A. Goldsmith, *Wireless Communications.* Cambridge, MA: Cambridge University Press, 2005.

[12] G. C. Goodwin, M. M. Seron and J. A. DeDona, *Constrained Control and Estimation - An Optimization Approach*. London, UK: Springer-Verlag, 2005.

[13] F.-S. Ho and P. Ioannou "Traffic flow modeling and control using artificial neural networks", *IEEE Control Systems*, vol. 16, no. 5, pp. 16-26, 1996.

[14] C.-Y. Kao and A. Rantzer, "Stability analysis of systems with uncertain time-varying delays", *Automatica*, vol. 43, no. 6, pp. 959-979, 2007.

[15] K. Lau, T. Wigren, R. Delgado and R. H. Middleton, "Disturbance rejection properties for a 5G networked data flow delay controller", *in Proc. CDC 2017*, pp. 1681-1687, Melbourne, Australia, Dec. 12-15, 2017.

[16] K. Lau, T. Wigren, R. H. Middleton and R. Delgado, "Delay alignment for 5G multi connectivity", *submitted* , 2018.

[17] A. Megretski and A. Rantzer, "System analysis via integral quadratic constraints", *IEEE Trans. Automat. Contr.*, vol. 42, no. 6, pp. 819-830, 1997.

[18] R. H. Middleton, T. Wigren, K. Lau and R. Delgado, "Data flow delay equalization for feedback control applications using 5G wireless dual connectivity", *Proc. VTC 2017 Spring*, Sydney, Australia, June 4-7, 2017.

[19] A. V. Oppenheim and R. W. Schafer, *Digital Signal Processing.* Englewood Cliffs, NJ: Prentice Hall, 1975.

[20] Y. Qian, H. Asplund, J.-E. Berg and Z. Guo, "Non-line-of-sight 2.6 GHz relay backhaul channel performance: field test and analysis", *Proc. VTC 2012-Fall*, Quebec City, Quebec, Canada, Sep. 3-6, 2012.

[21] T. S. Rappaport, R. W. Heath Jr., R. C. Daniels and J. N. Murdock, *Millimeter Wave Wireless Communications*. Westford, Massachusetts: Prencice Hall, 2014.

[22] T. Samad, "Control systems and the internet of things", *IEEE Control Systems*, vol. 36, no. 1, pp. 13-16, 2016.

[23] Technical Specification Group Radio Access Network; Scenarios and requirements for small cell enhancements for E-UTRA and E-UTRAN , 2015, 3GPP TS 36.321, release 12 (v. 12.2.0). [Online]. Available: http://www.3gpp.org/DynaReport/36322.htm

[24] Y. Song and J. Wang "Delay- and packet-disordering dependent H_∞ output tracking control for networked control systems", *Asian J. Contr.*, vol. 17, no. 3, pp. 917-931, 2015.

[25] R. Srikant and L. Ying, *Communication Networks - An Optimization, Control and Stochastic Networks Perspective*. Padstow Cornwall, UK: Cambridge Univeristy Press, 2014.

[26] M. Vidyasagar, *Nonlinear Systems Analysis*. Englewood Cliffs, NJ: Prentice-Hall, 1978.

[27] T. Wigren, "Robust $\mathcal{L}_2$ stable networked control of wireless packet queues over delayed internet connections", *IEEE Trans. Contr. Sys. Tech.*, vol. 24, no. 2, pp. 502-513, 2016. DOI: 10.1109/TCST.2015.2455933.

[28] T. Wigren, "Wireless feedback and feedforward data flow control subject to rate saturation and uncertain delay", *IET Control Theory & Applications*, vol. 10, no. 3, pp. 346-353, 2016. DOI: 10.1049/iet-cta.2015.0580.

[29] T. Wigren, "Low frequency sensitivity function constraints for nonlinear $\mathcal{L}_2$-stable networked control", *Asian J. Contr.*, vol. 18, no. 4, pp. 1200-1218, 2016. DOI: 10.1002/asjc.1241.

[30] T. Wigren, "Loop-shaping feedback and feedforward control for networked systems with saturation and delay", *Asian J. Contr.*, vol. 19, no. 4, pp. 1329-1349, 2017. DOI: 10.1002/asjc.1442.

[31] T. Wigren, D. Colombi, B. Thors and J. - E. Berg, "Implication of RF EMF exposure limitation on 5G data rates above 6 GHz", *IEEE VTC2015-Fall*, Boston, MA, September 6-9, 2015. DOI: 10.1109/VTC-Fall.2015.7390974.

Torbjörn Wigren (S'89-M'91-SM'98) received the M.Sc. degree (Engineering Physics) in 1985 and the Ph.D degree (Automatic Control) in 1990, from Uppsala University, Uppsala, Sweden, where he is now adjunct Professor of Automatic Control. He is employed by Ericsson AB, Stockholm, Sweden, where he works with signal processing and control for 5G wireless systems. In 2007, he received the Ericsson Inventor of the Year award. His main research interests include nonlinear identification, estimation and control for networked systems.

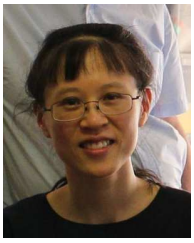

Katrina Lau (M'07) received her B.E. (Elec) in 1997, B.Math in 1999 and Ph.D in 2003 from The University of Newcastle, Australia. Since then, she has been a research academic working on a number of industrial projects. She is currently working on next generation control and telecommunications problems with Ericsson AB. Her other research interests include fundamental performance limitations, switched control systems and stability analysis.

Ramón A. Delgado received his professional title of Ingeniero Civil Electrónico and M.Sc. degree in Electronic Engineering from Universidad Técnica Federico Santa María, Chile, in 2009. He received the Ph.D. degree in Electrical Engineering from the University of Newcastle, Australia, in 2014. He is currently a research academic at the University of Newcastle. In his current role, Dr. Delgado is mainly focused on the current collaboration project between the University of Newcastle and the Swedish company Ericsson AB. His research interests include system identification, control, signal processing and optimisation.

Richard H. Middleton (S'84-M'86-SM'94-F'99) completed his Ph.D. (1987) from the University of Newcastle, Australia. He was a Research Professor at the Hamilton Institute, The National University of Ireland, Maynooth from May 2007 till 2011 and is currently Professor at the University of Newcastle and Head of the School of Electrical Engineering and Computing. He has served as Program Chair (CDC 2006), co-general chair (CDC 2017), CSS Vice President Membership Activities, and Vice President Conference Activities. In 2011, he was President of the IEEE Control Systems Society. He is a Fellow of IEEE and of IFAC, and his research interests include a broad range of Control Systems Theory and Applications, including Communications Systems, control of distributed systems and Systems Biology.